
RAQ-VAE: Rate-Adaptive Vector-Quantized Variational Autoencoder

Jiwan Seo, Joonhyuk Kang*

Department of Electrical Engineering

Korea Advanced Institute of Science and Technology (KAIST)

jeewan0516@kaist.ac.kr, jkang@kaist.ac.kr

Abstract

Vector Quantized Variational AutoEncoder (VQ-VAE) is an established technique in machine learning for learning discrete representations across various modalities. However, its scalability and applicability are limited by the need to retrain the model to adjust the codebook for different data or model scales. We introduce the Rate-Adaptive VQ-VAE (RAQ-VAE) framework, which addresses this challenge with two novel codebook representation methods: a model-based approach using a clustering-based technique on an existing well-trained VQ-VAE model, and a data-driven approach utilizing a sequence-to-sequence (Seq2Seq) model for variable-rate codebook generation. Our experiments demonstrate that RAQ-VAE achieves effective reconstruction performance across multiple rates, often outperforming conventional fixed-rate VQ-VAE models. This work enhances the adaptability and performance of VQ-VAEs, with broad applications in data reconstruction, generation, and computer vision tasks.

1 Introduction

Vector quantization (VQ) [14] is a fundamental technique for learning discrete representations for various tasks [23, 13, 50] in the field of machine learning. While preserving the encoder-decoder structure of a variational autoencoder (VAE) [22, 41], Vector Quantized Variational AutoEncoder (VQ-VAE) [48, 40] proposed so as to handle discrete latent representations. Learning discrete latent variable models with VQ-VAEs has shown promising results in computer vision [40, 11], audio [8, 59, 47], speech [25, 56], and other modalities [9, 58, 61] because data are inherently discrete, and these discrete representations are naturally suited to learning complex inference and prediction. Recently, there have been advancements of VQ-based discrete representation learning through the application of deep generative models, such as Generative Adversarial Networks (GANs) [11] and Denoising Diffusion Probabilistic Models (DDPMs) [5, 16, 59].

As VQ-VAE is integrated into diverse deep generative model frameworks, its utility and applicability in various tasks is becoming increasingly evident. However, even with this success, the *scalability* of the codebook-driven quantization process poses a significant challenge. With the proliferation of large datasets and the demand for real-time processing capabilities, traditional VQ-VAE architectures face limitations in accommodating the computational complexity associated with dynamic compression requirements, including the need to retrain the model when the user wants to increase or decrease the computational load. Consequently, addressing the *scalability* of the VQ process has become a crucial challenge in order to realize the full potential of VQ-VAE and integrate it with state-of-the-art generation model.

To address the issues, Li et al. [29] proposed a method to resize the codebook without retraining the publicly available VQ models by applying hyperbolic embeddings to enhance the codebook vector

*Corresponding author

with co-occurrence information and reordering the improved codebook with a Hilbert curve. Another approach to achieve more comprehensive codebook representation, the use of multi-codebook has been an ongoing challenge to achieve richer representations for different tasks [17]. Malka et al. [33] designed and learned a nested codebook based on progressive learning to support different quantization levels. Guo et al. [18] proposed a framework for predicting codebook indexes generated from embeddings of student models using multi-codebook vector quantization by reformulating teacher label generation as a codec problem in knowledge distillation. Recently, Huijben et al. [20] focused on unsupervised codebook generation based on residual quantization by studying the vector quantizer itself. However, addressing these issues through multi-codebook or residual quantization generally entails substantial changes to the existing well-established structure of VQ-VAEs, or face a reduction in the resolution of the quantized feature map.

To this end, we propose a Rate-Adaptive VQ-VAE (RAQ-VAE) framework that allows discrete representation at various rates with a single VQ-VAE model. First, we propose *model-based* RAQ-VAE that can use the existing VQ-VAE model to obtain rate-adaptive VQ through a differential k -means clustering (DKM) [3] algorithm and its inverse functionalization without any additional parameters and retraining. Next, we present *data-driven* RAQ-VAE with Sequence-to-Sequence (Seq2Seq) [44] model for rate-adaptive codebook generation. The *data-driven* RAQ-VAE can achieve discrete representation at any desired rate through the Seq2Seq model and approaches or partially outperforms the separately trained conventional VQ-VAE model. Our framework addresses the challenge of needing to train separate VQ-VAE models for different compression rates, especially in large computer vision tasks that demand high-capacity representations. Additionally, it can be seamlessly integrated into various VQ applications without requiring significant modifications to the existing VQ-VAE structure.

Our contributions are summarized as follows:

- We introduce the RAQ-VAE framework with two VQ codebook representation methods: *model-based* RAQ-VAE, utilizing an existing trained VQ-VAE model, and *data-driven* RAQ-VAE, combining Seq2Seq model with VQ-VAE architecture.
- We propose *model-based* RAQ-VAE, which adapts the codebook of a VQ-VAE model using a dynamic codebook clustering method, allowing the quantizer to adjust the rate without retraining.
- We propose *data-driven* RAQ-VAE, which generates a rate-adaptive codebook via Seq2Seq model. This method uses a single codebook and its training method, *cross-forcing*, to train recurrent networks to generate codebooks at different rates.
- Our experiments demonstrate that a single RAQ-VAE model achieves or even outperforms the performance of multiple conventional VQ-VAEs trained at fixed rates, using the same encoder-decoder architecture.

2 Background

Vector-Quantized Autoencoder VQ-VAEs [48, 40] can successfully represent meaningful features that span multiple dimensions of data space by discretizing continuous latent variables to the nearest code vector in its codebook. In VQ-VAE, learning of discrete representations is achieved by quantizing the encoded latent variables to their nearest neighbors in a trainable codebook and decoding the input data from the discrete latent variables. For discrete representations of $\mathbf{x} \in \mathcal{D}$ with the dataset \mathcal{D} , a codebook \mathbf{e} consisting of K learnable code vectors $\{e_i\}_{i=1}^K$ is used. The quantized discrete latent variable $\mathbf{z}_q(\mathbf{x}|\mathbf{e})$ is decoded to reconstruct the data \mathbf{x} . The quantizer Q modeled as deterministic categorical posterior maps a continuous latent representation $f_\phi(\mathbf{x})$ of the data \mathbf{x} by a deterministic encoder f_ϕ to $\mathbf{z}_q(\mathbf{x}|\mathbf{e})$ by finding the nearest neighbor in the D -dimensional codebook $\mathbf{e} = \{e_i\}_{i=1}^K$ as

$$\mathbf{z}_q(\mathbf{x}|\mathbf{e}) = Q(f_\phi(\mathbf{x})|\mathbf{e}) = \arg \min_{e_i \in \{e_i\}_{i=1}^K} \|f_\phi(\mathbf{x}) - e_i\|. \quad (1)$$

The quantized representation is **fixed** to $\log_2 K$ bits for the index i of the selected code vector e_i of the codebook of size K . The deterministic decoder f_θ reconstruct the data \mathbf{x} from the quantized discrete latent variable $\mathbf{z}_q(\mathbf{x}|\mathbf{e})$ as $\hat{\mathbf{x}} = f_\theta(\mathbf{z}_q(\mathbf{x}|\mathbf{e})|\mathbf{e})$. During the training process, the encoder f_ϕ ,

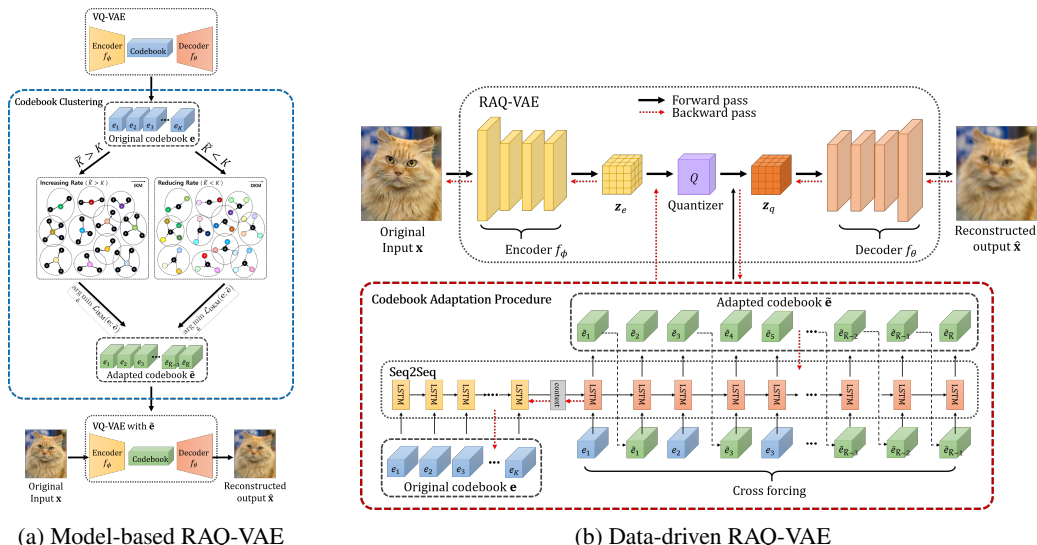


Figure 1: Our proposed RAQ-VAE framework: (i) model-based RAQ-VAE; (ii) data-driven RAQ-VAE. The model-based approach clusters the codebook \mathbf{e} of a trained VQ-VAE model with separate tasks for reducing and increasing to the adapted codebook $\tilde{\mathbf{e}}$ and applies it to the model. The data-driven approach trains a Seq2Seq-based codebook adaptation procedure utilizing the baseline VQ-VAE model with data, where the gradient flow of the codebook passes through the Seq2Seq model.

decoder f_θ , and codebook \mathbf{e} are jointly optimized to minimize the loss $\mathcal{L}_{\text{VQ}}(\phi, \theta; \mathbf{x}) =$

$$\underbrace{\log p_\theta(\mathbf{x}|\mathbf{z}_q(\mathbf{x};\mathbf{e}))}_{\mathcal{L}_{\text{recon}}} + \underbrace{\|\text{sg}[f_\phi(\mathbf{x})] - \mathbf{z}_q(\mathbf{x};\mathbf{e})\|_2^2}_{\mathcal{L}_{\text{embed}}} + \underbrace{\beta\|\text{sg}[\mathbf{z}_q(\mathbf{x};\mathbf{e})] - f_\phi(\mathbf{x})\|_2^2}_{\mathcal{L}_{\text{commit}}} \quad (2)$$

where $\text{sg}[\cdot]$ is the *stop-gradient* operator. The $\mathcal{L}_{\text{recon}}$ is the reconstruction loss between the input data \mathbf{x} and the reconstructed decoder output $\hat{\mathbf{x}}$. The two $\mathcal{L}_{\text{embed}}$ and $\mathcal{L}_{\text{commit}}$ apply only to codebook variables and encoder weight with a weighting hyperparameter β to prevent fluctuations from one code vector to another. Since the quantization process is non-differentiable, the codebook loss is typically approximated via a straight-through gradient estimator [1], such as $\partial\mathcal{L}/\partial f_\phi(\mathbf{x}) \approx \partial\mathcal{L}/\partial \mathbf{z}_q(\mathbf{x})$. Both conventional VAE [22] and VQ-VAE [48] have objective functions consisting of the sum of reconstruction error and latent regularization. To improve performance and convergence rate, exponential moving average (EMA) update is usually applied for the codebook optimization [48, 40] (for more details in supplementary material A.1).

Seq2Seq The sequence-to-sequence (Seq2Seq) [44] model is widely used in sequence prediction tasks such as language modeling and machine translation [7, 32, 39]. The model employs an initial LSTM, called the encoder, to process the input sequence sequentially and produce a substantial fixed-dimensional vector representation, called the context vector. The output sequence is then derived by a further LSTM, the decoder. In particular, the decoder is conditioned on the input sequence, distinguishing it as a distinct component within the architecture. During training, the Seq2Seq model typically uses *teacher forcing* [53], where the target sequence is provided to the decoder at each time step, instead of the decoder using its own previous output as input. This method helps the model converge faster by providing the correct context during training.

3 Rate-Adaptive VQ-VAE

Although VQ-VAE has been successfully applied to various domains, it still faces scalability limitation. In particular, the common fixed-rate VQ-VAE model requires modifying the codebook size K when processing different datasets (see [40, 11], using as many as 16384 and as few as 512 codebook sizes are used). Furthermore, adjusting the computational load requires retraining the model, which poses additional challenges. To overcome these limitations, we introduce two Rate-Adaptive VQ-VAE (RAQ-VAE) frameworks, which can adjust the rate of VQ-VAE through increasing or decreasing of the codebook size K . The outline of the RAQ-VAE framework is shown in Figure 1. RAQ-VAE

builds upon a codebook mapping $\Psi : (\mathbb{R}^D)^{\times K} \rightarrow (\mathbb{R}^D)^{\times \tilde{K}}$ for any integer $\tilde{K} \in \mathbb{N}$ that can be either lower, i.e., $\tilde{K} < K$, or higher, i.e., $\tilde{K} > K$, than the original codebook size K . We design the mapping in two ways: (i) model-based RAQ-VAE; (ii) data-driven RAQ-VAE. Model-based RAQ-VAE (Sec. 3.1) can obtain rate-adaptive VQ through differentiable k -means clustering (DKM) [3] algorithm without any additional parameters. In addition, data-driven RAQ-VAE (Sec. 3.2) is an offline-trained RAQ-VAE method that adopts the codebook generative Sequence-to-Sequence (Seq2Seq) [44] model.

3.1 Model-based Rate-Adaptive VQ-VAE

Previous attempts [27, 46, 62] have proposed enhancing codebook learning by periodically clustering the codebook during model training. In contrast, we propose a model-based rate-adaptive VQ-VAE that performs online codebook clustering after the model has been trained. By loading a VQ-VAE model trained with the original codebook \mathbf{e} and dynamically clustering the codebook to the adapted codebook $\tilde{\mathbf{e}}$. This allows the vector quantizer to adapt to nuanced patterns within the overall model, providing flexibility and scalability (See Figure 1a).

Codebook Clustering To achieve the desired rate for the adapted codebook size \tilde{K} ($= |\tilde{\mathbf{e}}|$), we derive the clustered codebook $\tilde{\mathbf{e}}$ from the original codebook \mathbf{e} . Details of the codebook clustering formulation are provided in supplementary material A.2. To ensure that the clustering process is effectively integrated into the trained VQ-VAE model, we employ a differentiable k -means clustering (DKM) algorithm [3]. This algorithm, originally proposed for DNN model compression, uses an attention-based weight clustering method. We adapt the DKM algorithm for VQ codebook clustering, focusing on the fine-tuning of clustered codebooks and VQ-VAE model architectures. Additionally, we utilize DKM for codebook incrementation (inverse functionalization process) to handle scenarios requiring an increase in codebook size.

Reducing the Rate ($\tilde{K} < K$) In the rate reduction task, DKM can perform iterative differentiable codebook clustering on \tilde{K} clusters. Let \mathbf{C} represent the cluster centers and vector \mathbf{e} represent the original codebook. The DKM algorithm [3] for VQ codebook operates as follows:

- Initialize a centroid $\mathbf{C} = \{c_j\}_{j=1}^{\tilde{K}}$ either by randomly selected \tilde{K} codebook vectors from \mathbf{e} or using k -means++. The last known \mathbf{C} from the previous batch is used for all following iterations.
- Calculate the distance between the original codebook vector e_i and initialized centroid c_j using Euclidean distance as the distance metric $d_{ij} = -f(e_i, c_j)$ with its matrix \mathbf{D} .
- To obtain the attention matrix \mathbf{A} , derive each row of \mathbf{A} where $a_{i,j} = \frac{\exp\left(\frac{d_{i,j}}{\tau}\right)}{\sum_k \exp\left(\frac{d_{i,k}}{\tau}\right)}$ represents the attention from e_i and c_j with a softmax temperature τ .
- Get a centroid candidate $\tilde{\mathbf{C}}$ by summing all the attentions for each centroid by computing $\tilde{c}_j = \frac{\sum_i a_{i,j} e_i}{\sum_i a_{i,j}}$ and update \mathbf{C} with $\tilde{\mathbf{C}}$.
- Repeat this process until $|\mathbf{C} - \tilde{\mathbf{C}}| \leq \epsilon$ at which point DKM has converged or the iteration limit reached, then compute \mathbf{AC} to get $\tilde{\mathbf{e}}$.

The above iterative process can be summarized as follows:

$$\tilde{\mathbf{e}} = \arg \min_{\tilde{\mathbf{e}}} \mathcal{L}_{\text{DKM}}(\mathbf{e}; \tilde{\mathbf{e}}) = \arg \min_{\mathbf{C}} |\mathbf{C} - \mathbf{AC}| = \arg \min_{\mathbf{C}} \sum_{j=1}^{\tilde{K}} \left| c_j - \frac{\sum_i a_{i,j} e_i}{\sum_i a_{i,j}} \right| \quad (3)$$

In [3], the authors implemented DKM for soft-weighted cluster assignment and hardness can be enforced to provide weighted clustering constraints. In the softmax operation, the temperature τ can be used to control the level of hardness. At the end of the DKM process, we use the last attention matrix \mathbf{A} to snap each codebook vector to the nearest centroid and finish clustering the codebook.

Increasing the Rate ($\tilde{K} > K$) While k -means clustering is effective for compressing code vectors, it has algorithmic limitations that prevent the augmentation of additional codebooks. To address this, we introduce the inverse functional DKM (IKM), a technique for increasing the number of codebooks. This iterative method aims to approximate the posterior distribution of an existing generated codebook. We use maximum mean discrepancy (MMD) to compare the distribution difference between the base codebook and the clustered generated codebook, where MMD is a kernel-based statistical test technique that measures the similarity between two distributions [15].

Assuming the original codebook vector \mathbf{e} of size K already trained in the baseline VQ-VAE, the process of generating the codebook $\tilde{\mathbf{e}}$ using the IKM algorithm is performed as follows:

- Initialize a D -dimensional adapted codebook vector $\tilde{\mathbf{e}} = \{\tilde{e}_i\}_{i=1}^{\tilde{K}}$ as $\tilde{\mathbf{e}} \sim \mathcal{N}(0, D^{-\frac{1}{2}}\mathbf{I})$
- Cluster $\tilde{\mathbf{e}}$ via the DKM process (equation 3): $g_{\text{DKM}}(\tilde{\mathbf{e}}) = \arg \min_{g_{\text{DKM}}(\tilde{\mathbf{e}})} \mathcal{L}_{\text{DKM}}(\tilde{\mathbf{e}}; g_{\text{DKM}}(\tilde{\mathbf{e}}))$.
- Calculate the MMD between the true original codebook \mathbf{e} and the DKM clustered $g_{\text{DKM}}(\tilde{\mathbf{e}})$.
- Optimize $\tilde{\mathbf{e}}$ to minimize the MMD objective $\mathcal{L}_{\text{IKM}}(\mathbf{e}; \tilde{\mathbf{e}}) = \text{MMD}(\mathbf{e}, g_{\text{DKM}}(\tilde{\mathbf{e}})) + \lambda \|\tilde{\mathbf{e}}\|_2^2$.

where λ is the regularization parameter controlling the strength of the L2 regularization term. The IKM process can be summarized as

$$\tilde{\mathbf{e}} = \arg \min_{\tilde{\mathbf{e}}} \mathcal{L}_{\text{IKM}}(\mathbf{e}; \tilde{\mathbf{e}}). \quad (4)$$

Since DKM does not block gradient flow, we easily can update the codebook $\tilde{\mathbf{e}}$ using stochastic gradient descent (SGD) as $\tilde{\mathbf{e}} = \mathbf{e} - \eta \nabla \mathcal{L}_{\text{IKM}}(\mathbf{e}, \tilde{\mathbf{e}})$.

With DKM and IKM, the generated codebook $\tilde{\mathbf{e}}$ can be used to quantize the encoded vector as $\mathbf{z}_q(\mathbf{x}|\tilde{\mathbf{e}})$ at different rates without adding any model parameters to the trained VQ-VAE. Since DKM does not block gradient flow, it is easy to change the codebook cluster assignments even during offline and online training. During offline training, the clusters that are best suited in terms of VQ task loss are adopted. Although we do not focus on using multi-codebook with DKM (aim to leverage rate-adaptive codebook after trained), a multi-codebook VQ-VAE model can be easily implemented by tuning \tilde{K} with DKM during training and hierarchically optimizing the multi-codebook clusters with the model.

3.2 Data-driven Rate-Adaptive VQ-VAE

Seq2Seq models [44] have been widely used in machine translation to handle variable output sequences, where the length of sentences can differ significantly between languages. Inspired by this, we propose a Seq2Seq-based approach to generate rate-adaptive codebooks within the VQ-VAE framework. This section introduces the data-driven RAQ-VAE, which integrates a learning vector quantization layer with Seq2Seq model.

Overview As shown in Figure 1b, data-driven RAQ-VAE is constructed with a deterministic encoder-decoder pair, a trainable original codebook \mathbf{e} , and Seq2Seq model. The adapted codebook $\tilde{\mathbf{e}}$ is generated by the Seq2Seq model from the original codebook \mathbf{e} . Data-driven RAQ-VAE hierarchically quantizes the continuous latent representation $f_\phi(x)$ of data \mathbf{x} into $\mathbf{z}_q(\mathbf{x}|\mathbf{e})$ and $\mathbf{z}_q(\mathbf{x}|\tilde{\mathbf{e}})$ via \mathbf{e} and $\tilde{\mathbf{e}}$, respectively. Building on the conventional VQ-VAE architecture, the data-driven RAQ-VAE learns the encoder-decoder pair while training the codebook \mathbf{e} and its generative process G_ψ .

Codebook Encoding The rate-adaptive codebook generation procedure, G_ψ , leverages LSTM cells in the Seq2Seq model to dynamically generate an adapted codebook $\tilde{\mathbf{e}}$ from the original codebook \mathbf{e} . The first step is to initialize the target codebook size \tilde{K} . During training, the data-driven RAQ-VAE is trained with arbitrary codebook sizes \tilde{K} . In the test phase, the Seq2Seq model generates the adapted codebook $\tilde{\mathbf{e}}$ at the desired rate specified by the user. This initialization sets the foundation for the encoding and decoding steps in Algorithm 1. Each vector of the original codebook e_i is sequentially encoded by a set of LSTM cells. The hidden and cell states (h, c) capture the contextual information of each base codebook vector.

Codebook Decoding via cross-forcing The goal of Seq2Seq codebook generation is to reflect as much information as possible from the original codebook while generating a usable codebook for the

VQ-VAE decoder. However, existing Seq2Seq training methods, such as teacher forcing [53], may not be suitable when the target adapted codebook $\tilde{\mathbf{e}}$ consists of sequences that are much longer than the original codebook. Therefore, we propose **cross-forcing**, a hybrid approach combining teacher forcing and free running in professor forcing [26]. This is feasible because, unlike typical sequence prediction tasks, the order of the codebooks does not significantly affect the outcome. In the decoding phase (as shown in Algorithm 1), teacher forcing is applied for odd steps that are less than twice the original codebook size ($2\tilde{K}$), using the base code vector (e_i) as input. For even steps and beyond, *free running* (using the previous time step decoder output as input) is performed to dynamically train the VQ-VAE decoder with the generated codebook.

Training Procedure To train the data-driven RAQ-VAE, we jointly optimize the base VQ-VAE and RAQ-VAE objectives to learn a good representation of the original codebook \mathbf{e} and the rate-adaptive codebook generative process G_ψ . We formulate the constrained optimization \mathcal{L}_{RAQ} to jointly update G_ψ with f_ϕ , f_θ , and \mathbf{e} as $\mathcal{L}_{\text{VQ}}(\phi, \theta, \mathbf{e}; \mathbf{x}) \geq \mathcal{L}_{\text{RAQ}}(\phi, \theta, \psi, \mathbf{e}; \mathbf{x}) =$

$$\log p_\theta(\mathbf{x}|\mathbf{z}_q(\mathbf{x}|G_\psi(\mathbf{e}))) + \|\text{sg}[f_\phi(\mathbf{x})] - \mathbf{z}_q(\mathbf{x}|G_\psi(\mathbf{e}))\|_2^2 + \beta \|\text{sg}[\mathbf{z}_q(\mathbf{x}|G_\psi(\mathbf{e}))] - f_\phi(\mathbf{x})\|_2^2. \quad (5)$$

where $\text{sg}[\cdot]$ is the *stop-gradient* operator. The data-driven RAQ-VAE jointly minimizes \mathcal{L}_{VQ} (equation 2) and \mathcal{L}_{RAQ} (equation 5). Back-propagating \mathcal{L}_{VQ} induces the same gradient flows as the base VQ-VAE. Additionally, back-propagating \mathcal{L}_{RAQ} induces a gradient flow to the Seq2Seq model, resulting in effective codebook generation. The overall training procedure for the proposed data-driven RAQ-VAE is summarized in Algorithm 2. During training, the Seq2Seq model dynamically generates codebooks and adapts to different rates at each training iteration.

Algorithm 1 Rate-adaptive codebook generation procedure G_ψ

Input: Original codebook $\mathbf{e} = \{e_i\}_{i=1}^K$
Output: Adapted codebook $\tilde{\mathbf{e}} = \{\tilde{e}_i\}_{i=1}^{\tilde{K}}$
Initialize adapted codebook size \tilde{K} ,
hidden $\mathbf{h} = \{h_i\}_{i=1}^K$ and cell $\mathbf{c} = \{c_i\}_{i=1}^K$
▷ Codebook encoding
for $i = 1$ **to** K **do**
 $h_i, c_i \leftarrow \text{LSTM}_\psi(e_i)$
end for
▷ Codebook decoding via *cross-forcing*
for $i = 1$ **to** \tilde{K} **do**
 if $i < 2K$ **and** i is odd **then**
 $\tilde{e}_i \leftarrow \text{LSTM}_\psi(e_i, h, c)$
 else
 $\tilde{e}_i \leftarrow \text{LSTM}_\psi(\tilde{e}_{i-1}, h, c)$
 end if
end for
Return: $\tilde{\mathbf{e}} = G_\psi(\mathbf{e})$

Algorithm 2 Training procedure of data-driven RAQ-VAE

Input: \mathbf{x} (batch of training data)
for $\mathbf{x} \in$ train dataset \mathcal{D} **do**
 ▷ Quantize encoder output $f_\phi(\mathbf{x})$ with \mathbf{e} .
 $\mathbf{z}_q(\mathbf{x}|\mathbf{e}) \leftarrow Q(f_\phi(\mathbf{x})|\mathbf{e})$
 ▷ Generate $\tilde{\mathbf{e}}$ from Seq2Seq model G_ψ .
 $\tilde{\mathbf{e}} \leftarrow G_\psi(\mathbf{e})$ by Algorithm 1
 ▷ Quantize encoder output $f_\phi(\mathbf{x})$ with $\tilde{\mathbf{e}}$.
 $\mathbf{z}_q(\mathbf{x}|\tilde{\mathbf{e}}) \leftarrow Q(f_\phi(\mathbf{x})|\tilde{\mathbf{e}})$
 $\hat{\mathbf{x}}_{\mathbf{e}}, \hat{\mathbf{x}}_{\tilde{\mathbf{e}}} \leftarrow f_\theta(\mathbf{z}_q(\mathbf{x}|\mathbf{e})), f_\theta(\mathbf{z}_q(\mathbf{x}|\tilde{\mathbf{e}}))$
 Compute \mathcal{L}_{VQ} by equation 2.
 Compute \mathcal{L}_{RAQ} by equation 5.
 $\phi, \theta, \mathbf{e} \leftarrow \text{Update}(\mathcal{L}_{\text{VQ}})$
 $\phi, \theta, \psi, \mathbf{e} \leftarrow \text{Update}(\mathcal{L}_{\text{RAQ}})$
end for
Return: $f_\phi, f_\theta, G_\psi, \mathbf{e}$

4 Related Work

VQ-VAE and its Improvements The VQ-VAE [48] has inspired numerous developments since its inception. Łańcucki et al. [27], Williams et al. [54], Zheng and Vedaldi [62] proposed codeword reset and online clustering methods to address the problem of *codebook collapse* [45], thereby increasing the training efficiency of the codebook. Tjandra et al. [46] introduced a conditional VQ-VAE that generates magnitude spectrograms for target speech using a multi-scale codebook-to-spectrogram inverter given the VQ-VAE codebook. SQ-VAE [45] incorporated stochastic quantization and a trainable posterior categorical distribution to enhance VQ-VAE performance, while Vuong et al. [51] proposed VQ-WAE, based on SQ-VAE, using Wasserstein distance to ensure a uniform distribution of discrete representations. Several works have introduced substantial structural changes to VQ-VAE. Lee et al. [28] proposed a two-step framework with Residual Quantized (RQ) VAE and RQ-Transform to generate high-resolution images using a single shared codebook. Mentzer et al. [34] replaced VQ with Finite Scalar Quantization (FSQ) to tackle codebook collapse. However, unlike previous works, we focus on achieving rate-adaptive VQ-VAE within a largely unchanged quantization scheme and

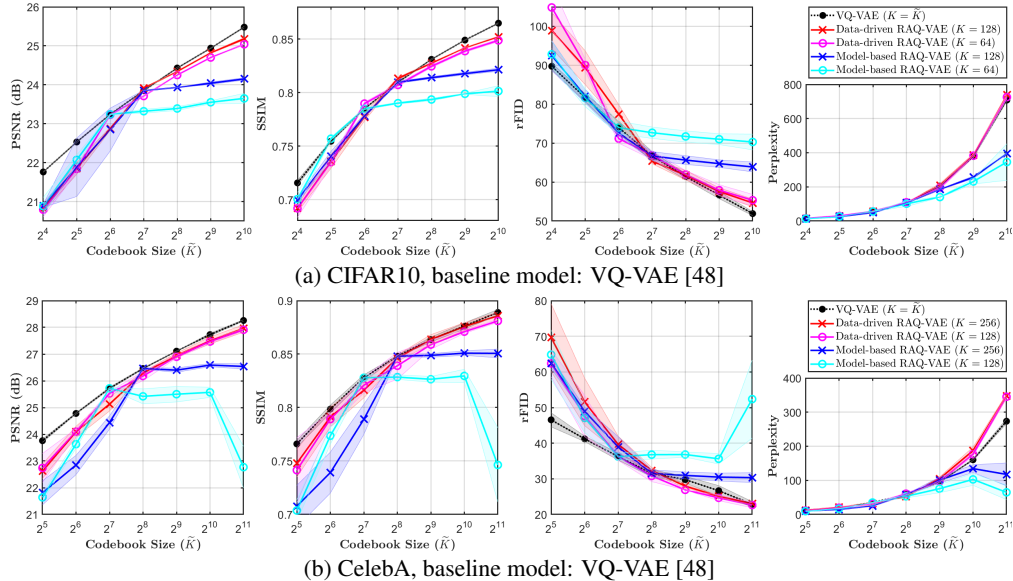


Figure 2: **Reconstruction performance** at different rates (adapted codebook sizes) evaluated on (a) CIFAR-10 and (b) CelebA. Higher values are better for PSNR, SSIM, and perplexity, while lower values are better for rFID. In the graph, the black VQ-VAEs are separate models trained on each codebook size, while the RAQ-VAEs are one model per line. The shaded area indicates the 95.45% confidence interval based on 4 runs with different training seeds.

VQ-VAE model architecture to improve its scalability for application not only to basic VQ-VAE models but also to its advanced models.

Variable-Rate Neural Image Compression Several studies have proposed variable-rate learning image compression frameworks based on different neural network architectures. Yang et al. [60], Choi et al. [4], Cui et al. [6] introduced frameworks based on autoencoders, conditional autoencoders, and VAE structures, respectively. Variable-rate image compression has also been achieved in studies such as Song et al. [43], which uses models based on the Spatial Feature Transform (SFT) for compression, and Johnston et al. [21], which employs recurrent neural networks (RNNs) to achieve variable-rate compression by evaluating the distortion of individual patches to compute a weighted distortion. Duong et al. [10] proposed learned transforms and entropy coding to enhance the linear transforms in existing codecs by systematizing the process into a single model that follows the rate-distortion curve. However, the integration of variable-rate image compression within the VQ-VAE framework remains an open question. Unlike these studies, our work focuses on embedding variable-rate compression directly into the VQ-VAE framework, maintaining the benefits of VQ while enhancing scalability and adaptability.

5 Experiments

Implementation To demonstrate the advancement of the proposed RAQ-VAE, we adapt the conventional VQ-VAE [48] and the two-level hierarchical VQ-VAE (VQ-VAE-2) [40] as baselines. We perform empirical evaluations on vision datasets: CIFAR10 (32×32) [24] and CelebA (64×64) [30] for quantitative evaluation, and ImageNet (256×256) [42] for qualitative evaluation. We designed RAQ-VAE to adapt the conventional VQ-VAE and its improved model structures [46, 35, 11, 38] to achieve multiple rates within a single model.

Architecture We use identical architecture and parameters for all methods, setting the default codeword (discrete latent) embedding dimension D to 64 for CIFAR10 and CelebA, and to 128 for ImageNet. The codebook sizes range from 16 to 1024 for CIFAR10, 32 to 2048 for CelebA, and 128 to 4096 for ImageNet, with conventional VQ-VAE models trained on 'power of 2' sizes and RAQ-VAE models set to the middle of the range for both model-based and data-driven approaches. Details of the experimental settings are provided in supplementary material A.3.

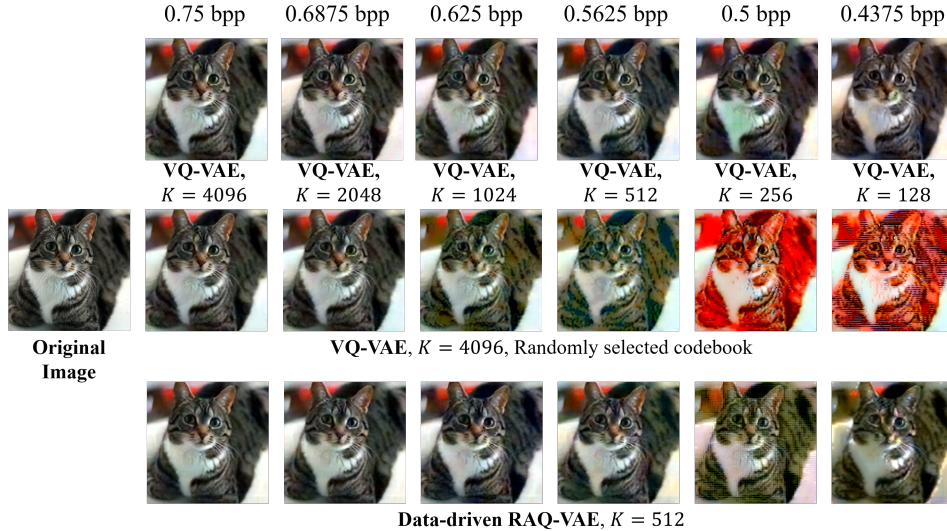


Figure 3: **Reconstructed images** for ImageNet dataset at different rates.

Evaluation Metrics We quantitatively evaluated our method using peak-signal-to-noise-ratio (PSNR), structural similarity index measure (SSIM), reconstructed Fréchet inception distance (rFID) [19], and codebook perplexity. PSNR measures the ratio between the maximum possible power of a signal and the power of the corrupted noise affecting data fidelity. SSIM assesses structural similarity between two images [52]. rFID evaluates the reconstructed image quality on the test data and is highly correlated with human perceptual judgment. Codebook perplexity, defined as $e^{-\sum_i^K p_{e_i} \log p_{e_i}}$ where $p_{e_i} = \frac{N_{e_i}}{\sum_j^K N_{e_j}}$ and N_{e_i} represents the encoded number for latent representation with codebook e_i , indicates a uniform prior distribution when the perplexity value reaches the codebook size (\tilde{K}), meaning all codebooks are used equally.

5.1 Main Results on Vision Tasks

Quantitative Evaluation We empirically compare our RAQ-VAE models with the conventional VQ-VAE [48] for image reconstruction performance. We trained and evaluated each VQ-VAE with different codebook sizes (K) as a quantitative baseline, and then validated RAQ-VAE by adapting the rate (by adjusting \tilde{K}) on a single model-based and data-driven RAQ-VAE model. Figure 2 shows the results, evaluated on the CIFAR10 and CelebA datasets. Under same compression rate and network architecture, all proposed RAQ-VAE models achieve performance close to that of multiple VQ-VAE models. When increasing the rate (codebook size), the data-driven RAQ-VAE achieves slightly lower results for the PSNR and SSIM metrics but significantly better results in terms of rFID score, which evaluates perceptual image quality at the dataset level. In particular, the perplexity of the conventional VQ-VAE models shows low scores on CelebA, but the proposed data-driven RAQ-VAE performs better in terms of perplexity and rFID, especially at high bits per pixel (bpp). The model-based RAQ-VAE performs poorly overall, but in the task of reducing the rate, it achieves intermittently more reliable results on CIFAR10. Our proposed method is highly portable and reduces model complexity, considering the resources invested in each single VQ-VAE, since RAQ-VAE covers multiple fixed-rate VQ-VAE models with only a single model. (The number of parameters of baseline VQ-VAEs and RAQ-VAEs are provided in A.3.3.)

Qualitative Evaluation For qualitative evaluation, we compare VQ-VAEs and a single data-driven RAQ-VAE trained at different rates (0.4375 bpp to 0.75 bpp) on ImageNet (256×256). In Figure 3, the VQ-VAEs (in the first row) are trained for each rate and show that the quality decreases as the rate decreases, which is consistent with the results observed in the quantitative evaluation. If we randomly select the codebook of the VQ-VAE model trained with $K = 4096$ (in the second row) to reduce the rate, the color changes compared to the original image, and from 0.5 bpp, the image is reconstructed with a similar shape but a different color in the red family. However, the data-driven RAQ-VAE with a low bpp ($K = 512$) original codebook (in the third row) preserves the high-level semantic features

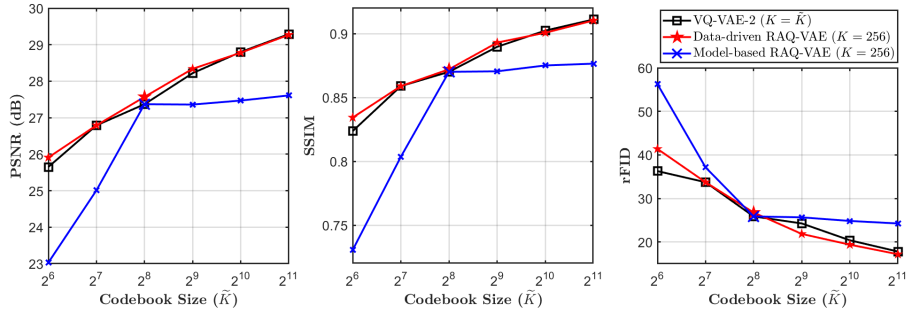


Figure 4: **Reconstruction performance** at different rates (adapted codebook sizes) evaluated on CelebA test set. In the graph, the black VQ-VAE-2s [40] are separate models trained on each codebook size, while the RAQ-VAEs are one model per line.

and colors of the input image well with only a single model trained on the low-rate base codebook (0.5625 bpp). In particular, it recovers the fine details of the image (such as the cat’s whiskers) much better than the results where the codebook was randomly selected. Although the overall image quality and tone are reduced at the lowest bpp compared to the original, it is possible to enhance image generation quality when the discrete representations are combined with state-of-the-art PixelCNN [49] or PixelSNAIL [2] as the prior estimator and fed to the VQ decoder, as shown in most VQ-VAE studies [48, 40, 11]. See supplementary material A.4.3 for more image reconstruction samples.

5.2 Detailed Analysis

Codebook Usability Following the observations of previous works [55, 45, 51], we note that as the codebook size increases, the codebook perplexity of data-driven RAQ-VAE also increases, leading to better reconstruction performance. In most VQ-VAE frameworks, codebook perplexity is considered optimal when it approaches the codebook size, effectively utilizing the available resources when the codebook size is limited. As demonstrated in the main quantitative evaluation (see Figure 2), the data-driven RAQ-VAE outperforms conventional VQ-VAE in terms of codebook perplexity at higher bits per pixel (bpp). This improvement highlights the effectiveness of the Seq2Seq model in generating a codebook that the decoder can consistently and efficiently utilize. The ability of data-driven RAQ-VAE to maintain high codebook perplexity ensures better representation and reconstruction quality, proving its robustness in handling larger codebooks.

Rate Adaptation To demonstrate the rate adaptation performance, we validated RAQ-VAE by varying the adapted codebook size (\tilde{K}). For the rate reduction task ($\tilde{K} < K$), our experiments show that data-driven RAQ-VAE generally outperforms model-based RAQ-VAE in most aspects. However, on the CIFAR10, the model-based RAQ-VAE performs better at some rates. When a VQ-VAE model achieves high codebook perplexity, substantial performance can be achieved by simply clustering the codebook vectors (see more results in supplementary material A.4.1). For the rate increasing task ($\tilde{K} > K$), a more challenging adaptation task, data-driven RAQ-VAE successfully generated higher-rate codebooks, outperforming model-based RAQ-VAE and partially surpassing conventional VQ-VAE models trained at the same codebook size. This capability was especially pronounced on the CelebA dataset. However, for model-based RAQ-VAE, increasing the difference between the original and adjusted codebook sizes resulted in noticeable performance degradation, exposing the limitations of the current implementation.

Applicability To demonstrate the broader applicability of our methodology, we extend our approach to the two-level hierarchical VQ-VAE (VQ-VAE-2) [40]. The VQ-VAE-2 model builds on the original VQ-VAE framework by incorporating a hierarchical structure that allows for improved representation and reconstruction capabilities. Figure 4 shows the reconstruction performance using VQ-VAE-2 as the baseline model. The results demonstrate that the data-driven RAQ-VAE model significantly outperforms the original VQ-VAE-2 across multiple rates on the CelebA dataset. In particular, under the same original codebooks size, the VQ-VAE-2 parameters is about 2 times higher than VQ-VAE, but the hierarchical structure of VQ-VAE-2 enables it to capture more nuanced features of the data, improving the overall reconstruction quality. By applying our rate-adaptive quantization method to VQ-VAE-2, we found that it not only achieved the improved performance of the hierarchical model

but also provided the flexibility to adapt to different rates without retraining the entire model. This indicates that our approach is not limited to the VQ-VAE but can be effectively applied to more advanced versions such as VQ-VAE-2, highlighting its versatility and robustness in various VQ-VAE frameworks. The ability to seamlessly integrate with and extend VQ-VAE models such as VQ-VAE-2 underscores the potential of our RAQ-VAE framework for broader applications in data reconstruction and generation tasks.

6 Conclusion

We introduced the Rate-Adaptive VQ-VAE (RAQ-VAE) framework, addressing the scalability limitations of conventional VQ-VAEs by enabling dynamic adjustment of the codebook size. Our experiments demonstrate that RAQ-VAE achieves superior reconstruction performance across multiple rates without retraining. This rate-adaptive feature provides flexibility in applications requiring dynamic compression levels, such as variable-rate image/video compression and real-time end-to-end communication systems [57, 36]. With its demonstrated versatility, RAQ-VAE has the potential to significantly advance both theoretical and practical aspects of machine learning.

References

- [1] Yoshua Bengio, Nicholas Léonard, and Aaron Courville. Estimating or propagating gradients through stochastic neurons for conditional computation. *arXiv preprint arXiv:1308.3432*, 2013.
- [2] XI Chen, Nikhil Mishra, Mostafa Rohaninejad, and Pieter Abbeel. PixelSNAIL: An improved autoregressive generative model. In Jennifer Dy and Andreas Krause, editors, *Proceedings of the 35th International Conference on Machine Learning*, volume 80 of *Proceedings of Machine Learning Research*, pages 864–872. PMLR, 10–15 Jul 2018.
- [3] Minsik Cho, Keivan Alizadeh-Vahid, Saurabh Adya, and Mohammad Rastegari. Dkm: Differentiable k-means clustering layer for neural network compression. In *International Conference on Learning Representations*, 2021.
- [4] Yoojin Choi, Mostafa El-Khamy, and Jungwon Lee. Variable rate deep image compression with a conditional autoencoder. In *Proceedings of the IEEE/CVF International Conference on Computer Vision*, pages 3146–3154, 2019.
- [5] Max Cohen, Guillaume Quispe, Sylvain Le Corff, Charles Ollion, and Eric Moulines. Diffusion bridges vector quantized variational autoencoders. In Kamalika Chaudhuri, Stefanie Jegelka, Le Song, Csaba Szepesvari, Gang Niu, and Sivan Sabato, editors, *Proceedings of the 39th International Conference on Machine Learning*, volume 162 of *Proceedings of Machine Learning Research*, pages 4141–4156. PMLR, 17–23 Jul 2022. URL <https://proceedings.mlr.press/v162/cohen22b.html>.
- [6] Ze Cui, Jing Wang, Bo Bai, Tiansheng Guo, and Yihui Feng. G-vae: A continuously variable rate deep image compression framework. *arXiv preprint arXiv:2003.02012*, 2(3), 2020.
- [7] Andrew M Dai and Quoc V Le. Semi-supervised sequence learning. *Advances in neural information processing systems*, 28, 2015.
- [8] Prafulla Dhariwal, Heewoo Jun, Christine Payne, Jong Wook Kim, Alec Radford, and Ilya Sutskever. Jukebox: A generative model for music. *arXiv preprint arXiv:2005.00341*, 2020.
- [9] Ming Ding, Zhuoyi Yang, Wenyi Hong, Wendi Zheng, Chang Zhou, Da Yin, Junyang Lin, Xu Zou, Zhou Shao, Hongxia Yang, et al. Cogview: Mastering text-to-image generation via transformers. *Advances in Neural Information Processing Systems*, 34:19822–19835, 2021.
- [10] Lyndon R Duong, Bohan Li, Cheng Chen, and Jingning Han. Multi-rate adaptive transform coding for video compression. In *ICASSP 2023-2023 IEEE International Conference on Acoustics, Speech and Signal Processing (ICASSP)*, pages 1–5. IEEE, 2023.
- [11] Patrick Esser, Robin Rombach, and Bjorn Ommer. Taming transformers for high-resolution image synthesis. In *Proceedings of the IEEE/CVF conference on computer vision and pattern recognition*, pages 12873–12883, 2021.

- [12] William A Falcon. Pytorch lightning. *GitHub*, 3, 2019.
- [13] Yunchao Gong, Liu Liu, Ming Yang, and Lubomir Bourdev. Compressing deep convolutional networks using vector quantization. *arXiv preprint arXiv:1412.6115*, 2014.
- [14] Robert Gray. Vector quantization. *IEEE Assp Magazine*, 1(2):4–29, 1984.
- [15] Arthur Gretton, Karsten M Borgwardt, Malte J Rasch, Bernhard Schölkopf, and Alexander Smola. A kernel two-sample test. *The Journal of Machine Learning Research*, 13(1):723–773, 2012.
- [16] Shuyang Gu, Dong Chen, Jianmin Bao, Fang Wen, Bo Zhang, Dongdong Chen, Lu Yuan, and Baining Guo. Vector quantized diffusion model for text-to-image synthesis. In *Proceedings of the IEEE/CVF Conference on Computer Vision and Pattern Recognition*, pages 10696–10706, 2022.
- [17] Haohan Guo, Fenglong Xie, Frank K Soong, Xixin Wu, and Helen Meng. A multi-stage multi-codebook vq-vae approach to high-performance neural tts. In *Proc. INTERSPEECH*, 2022.
- [18] Liyong Guo, Xiaoyu Yang, Quandong Wang, Yuxiang Kong, Zengwei Yao, Fan Cui, Fangjun Kuang, Wei Kang, Long Lin, Mingshuang Luo, et al. Predicting multi-codebook vector quantization indexes for knowledge distillation. In *ICASSP 2023-2023 IEEE International Conference on Acoustics, Speech and Signal Processing (ICASSP)*, pages 1–5. IEEE, 2023.
- [19] Martin Heusel, Hubert Ramsauer, Thomas Unterthiner, Bernhard Nessler, and Sepp Hochreiter. Gans trained by a two time-scale update rule converge to a local nash equilibrium. *Advances in neural information processing systems*, 30, 2017.
- [20] Iris Huijben, Matthijs Douze, Matthew Muckley, Ruud van Sloun, and Jakob Verbeek. Residual quantization with implicit neural codebooks. *arXiv preprint arXiv:2401.14732*, 2024.
- [21] Nick Johnston, Damien Vincent, David Minnen, Michele Covell, Saurabh Singh, Troy Chinen, Sung Jin Hwang, Joel Shor, and George Toderici. Improved lossy image compression with priming and spatially adaptive bit rates for recurrent networks. In *Proceedings of the IEEE conference on computer vision and pattern recognition*, pages 4385–4393, 2018.
- [22] Diederik P Kingma and Max Welling. Auto-encoding variational bayes. *arXiv preprint arXiv:1312.6114*, 2013.
- [23] Ashok K. Krishnamurthy, Stanley C. Ahalt, Douglas E. Melton, and Prakoon Chen. Neural networks for vector quantization of speech and images. *IEEE journal on selected areas in Communications*, 8(8):1449–1457, 1990.
- [24] Alex Krizhevsky, Geoffrey Hinton, et al. Learning multiple layers of features from tiny images. 2009.
- [25] Kundan Kumar, Rithesh Kumar, Thibault De Boissiere, Lucas Gestin, Wei Zhen Teoh, Jose Sotelo, Alexandre De Brebisson, Yoshua Bengio, and Aaron C Courville. Melgan: Generative adversarial networks for conditional waveform synthesis. *Advances in neural information processing systems*, 32, 2019.
- [26] Alex M Lamb, Anirudh Goyal ALIAS PARTH GOYAL, Ying Zhang, Saizheng Zhang, Aaron C Courville, and Yoshua Bengio. Professor forcing: A new algorithm for training recurrent networks. *Advances in neural information processing systems*, 29, 2016.
- [27] Adrian Łańcucki, Jan Chorowski, Guillaume Sanchez, Ricard Marxer, Nanxin Chen, Hans JGA Dolfing, Sameer Khurana, Tanel Alumäe, and Antoine Laurent. Robust training of vector quantized bottleneck models. In *2020 International Joint Conference on Neural Networks (IJCNN)*, pages 1–7. IEEE, 2020.
- [28] Doyup Lee, Chiheon Kim, Saehoon Kim, Minsu Cho, and Wook-Shin Han. Autoregressive image generation using residual quantization. In *Proceedings of the IEEE/CVF Conference on Computer Vision and Pattern Recognition*, pages 11523–11532, 2022.

- [29] Lei Li, Tingting Liu, Chengyu Wang, Minghui Qiu, Cen Chen, Ming Gao, and Aoying Zhou. Resizing codebook of vector quantization without retraining. *Multimedia Systems*, 29(3): 1499–1512, 2023.
- [30] Ziwei Liu, Ping Luo, Xiaogang Wang, and Xiaoou Tang. Deep learning face attributes in the wild. In *Proceedings of International Conference on Computer Vision (ICCV)*, December 2015.
- [31] Ilya Loshchilov and Frank Hutter. Decoupled weight decay regularization. In *7th International Conference on Learning Representations, ICLR 2019, New Orleans, LA, USA, May 6-9, 2019*. OpenReview.net, 2019. URL <https://openreview.net/forum?id=Bkg6RiCqY7>.
- [32] Minh-Thang Luong, Quoc V. Le, Ilya Sutskever, Oriol Vinyals, and Lukasz Kaiser. Multi-task sequence to sequence learning. In Yoshua Bengio and Yann LeCun, editors, *4th International Conference on Learning Representations, ICLR 2016, San Juan, Puerto Rico, May 2-4, 2016, Conference Track Proceedings*, 2016. URL <http://arxiv.org/abs/1511.06114>.
- [33] May Malka, Shai Ginzach, and Nir Shlezinger. Learning multi-rate vector quantization for remote deep inference. In *2023 IEEE International Conference on Acoustics, Speech, and Signal Processing Workshops (ICASSPW)*, pages 1–5. IEEE, 2023.
- [34] Fabian Mentzer, David Minnen, Eirikur Agustsson, and Michael Tschannen. Finite scalar quantization: Vq-vae made simple. *arXiv preprint arXiv:2309.15505*, 2023.
- [35] Myle Ott, Sergey Edunov, Alexei Baevski, Angela Fan, Sam Gross, Nathan Ng, David Grangier, and Michael Auli. fairseq: A fast, extensible toolkit for sequence modeling. In *Proceedings of NAACL-HLT 2019: Demonstrations*, 2019.
- [36] Sangwoo Park, Osvaldo Simeone, and Joonhyuk Kang. Meta-learning to communicate: Fast end-to-end training for fading channels. In *ICASSP 2020-2020 IEEE International Conference on Acoustics, Speech and Signal Processing (ICASSP)*, pages 5075–5079. IEEE, 2020.
- [37] Adam Paszke, Sam Gross, Francisco Massa, Adam Lerer, James Bradbury, Gregory Chanan, Trevor Killeen, Zeming Lin, Natalia Gimelshein, Luca Antiga, et al. Pytorch: An imperative style, high-performance deep learning library. *Advances in neural information processing systems*, 32, 2019.
- [38] Aditya Ramesh, Mikhail Pavlov, Gabriel Goh, Scott Gray, Chelsea Voss, Alec Radford, Mark Chen, and Ilya Sutskever. Zero-shot text-to-image generation. In *International Conference on Machine Learning*, pages 8821–8831. PMLR, 2021.
- [39] Marc’Aurelio Ranzato, Sumit Chopra, Michael Auli, and Wojciech Zaremba. Sequence level training with recurrent neural networks. In Yoshua Bengio and Yann LeCun, editors, *4th International Conference on Learning Representations, ICLR 2016, San Juan, Puerto Rico, May 2-4, 2016, Conference Track Proceedings*, 2016. URL <http://arxiv.org/abs/1511.06732>.
- [40] Ali Razavi, Aaron Van den Oord, and Oriol Vinyals. Generating diverse high-fidelity images with vq-vae-2. *Advances in neural information processing systems*, 32, 2019.
- [41] Danilo Jimenez Rezende and Fabio Viola. Taming vaes. *arXiv preprint arXiv:1810.00597*, 2018.
- [42] Olga Russakovsky, Jia Deng, Hao Su, Jonathan Krause, Sanjeev Satheesh, Sean Ma, Zhiheng Huang, Andrej Karpathy, Aditya Khosla, Michael Bernstein, Alexander C. Berg, and Li Fei-Fei. ImageNet Large Scale Visual Recognition Challenge. *International Journal of Computer Vision (IJCV)*, 115(3):211–252, 2015. doi: 10.1007/s11263-015-0816-y.
- [43] Myungseo Song, Jinyoung Choi, and Bohyung Han. Variable-rate deep image compression through spatially-adaptive feature transform. In *Proceedings of the IEEE/CVF International Conference on Computer Vision*, pages 2380–2389, 2021.
- [44] Ilya Sutskever, Oriol Vinyals, and Quoc V Le. Sequence to sequence learning with neural networks. *Advances in neural information processing systems*, 27, 2014.

- [45] Yuhta Takida, Takashi Shibuya, Weihsiang Liao, Chieh-Hsin Lai, Junki Ohmura, Toshimitsu Uesaka, Naoki Murata, Shusuke Takahashi, Toshiyuki Kumakura, and Yuki Mitsufuji. Sq-vae: Variational bayes on discrete representation with self-annealed stochastic quantization. In *International Conference on Machine Learning*, pages 20987–21012. PMLR, 2022.
- [46] Andros Tjandra, Berrak Sisman, Mingyang Zhang, Sakriani Sakti, Haizhou Li, and Satoshi Nakamura. Vqvae unsupervised unit discovery and multi-scale code2spec inverter for zerospeech challenge 2019. *arXiv preprint arXiv:1905.11449*, 2019.
- [47] Jonathan Tseng, Rodrigo Castellon, and Karen Liu. Edge: Editable dance generation from music. In *Proceedings of the IEEE/CVF Conference on Computer Vision and Pattern Recognition*, pages 448–458, 2023.
- [48] Aaron Van Den Oord, Oriol Vinyals, et al. Neural discrete representation learning. *Advances in neural information processing systems*, 30, 2017.
- [49] Aäron van den Oord, Nal Kalchbrenner, and Koray Kavukcuoglu. Pixel recurrent neural networks. In Maria Florina Balcan and Kilian Q. Weinberger, editors, *Proceedings of The 33rd International Conference on Machine Learning*, volume 48 of *Proceedings of Machine Learning Research*, pages 1747–1756, New York, New York, USA, 20–22 Jun 2016. PMLR. URL <https://proceedings.mlr.press/v48/oord16.html>.
- [50] Benjamin Van Niekerk, Leanne Nortje, and Herman Kamper. Vector-quantized neural networks for acoustic unit discovery in the zerospeech 2020 challenge. *arXiv preprint arXiv:2005.09409*, 2020.
- [51] Tung-Long Vuong, Trung Le, He Zhao, Chuanxia Zheng, Mehrtash Harandi, Jianfei Cai, and Dinh Phung. Vector quantized wasserstein auto-encoder. *arXiv preprint arXiv:2302.05917*, 2023.
- [52] Zhou Wang, Alan C Bovik, Hamid R Sheikh, and Eero P Simoncelli. Image quality assessment: from error visibility to structural similarity. *IEEE transactions on image processing*, 13(4): 600–612, 2004.
- [53] Ronald J Williams and David Zipser. A learning algorithm for continually running fully recurrent neural networks. *Neural computation*, 1(2):270–280, 1989.
- [54] Will Williams, Sam Ringer, Tom Ash, David MacLeod, Jamie Dougherty, and John Hughes. Hierarchical quantized autoencoders. *Advances in Neural Information Processing Systems*, 33: 4524–4535, 2020.
- [55] Hanwei Wu and Markus Flierl. Vector quantization-based regularization for autoencoders. In *Proceedings of the AAAI Conference on Artificial Intelligence*, volume 34, pages 6380–6387, 2020.
- [56] Jinbo Xing, Menghan Xia, Yuechen Zhang, Xiaodong Cun, Jue Wang, and Tien-Tsin Wong. Codetalker: Speech-driven 3d facial animation with discrete motion prior. In *Proceedings of the IEEE/CVF Conference on Computer Vision and Pattern Recognition*, pages 12780–12790, 2023.
- [57] Jialong Xu, Tze-Yang Tung, Bo Ai, Wei Chen, Yuxuan Sun, and Deniz Deniz Gündüz. Deep joint source-channel coding for semantic communications. *IEEE Communications Magazine*, 61(11):42–48, 2023.
- [58] Wilson Yan, Yunzhi Zhang, Pieter Abbeel, and Aravind Srinivas. Videogpt: Video generation using vq-vae and transformers. *arXiv preprint arXiv:2104.10157*, 2021.
- [59] Dongchao Yang, Jianwei Yu, Helin Wang, Wen Wang, Chao Weng, Yuexian Zou, and Dong Yu. Diffsound: Discrete diffusion model for text-to-sound generation. *IEEE/ACM Transactions on Audio, Speech, and Language Processing*, 2023.
- [60] Fei Yang, Luis Herranz, Joost Van De Weijer, José A Iglesias Guitián, Antonio M López, and Mikhail G Mozerov. Variable rate deep image compression with modulated autoencoder. *IEEE Signal Processing Letters*, 27:331–335, 2020.

- [61] Jianrong Zhang, Yangsong Zhang, Xiaodong Cun, Shaoli Huang, Yong Zhang, Hongwei Zhao, Hongtao Lu, and Xi Shen. T2m-gpt: Generating human motion from textual descriptions with discrete representations. *arXiv preprint arXiv:2301.06052*, 2023.
- [62] Chuanxia Zheng and Andrea Vedaldi. Online clustered codebook. In *Proceedings of the IEEE/CVF International Conference on Computer Vision*, pages 22798–22807, 2023.

A Appendix / Supplementary Material

A.1 VQ-VAE codebook updates with Exponential Moving Averages (EMA)

At training step t , the n_i encoder outputs $\{f_\phi(x_1), f_\phi(x_2), \dots, f_\phi(x_{n_i})\}$ from codebook e_i for the mini-batch data $\{x_1, x_2, \dots, x_{n_i}\}$ are updated with count $N_i^{(t)}$ and mean value $m_i^{(t)}$ as follows:

$$\begin{aligned} N_i^{(t)} &:= \gamma \cdot N_i^{(t-1)} + (1 - \gamma) \cdot n_i^{(t)} \\ m_i^{(t)} &:= \gamma \cdot m_i^{(t-1)} + (1 - \gamma) \cdot \sum_j^{n_i^{(t)}} f_\phi(x_j)^{(t)} \\ e_i^{(t)} &:= \frac{m_i^{(t)}}{N_i^{(t)}} \end{aligned} \tag{6}$$

where a γ is a decay factor with a value between 0 and 1 (the default value $\gamma = 0.99$ was used in all of our experiments). The count $N_i^{(t)}$ represents the encoder hidden states that have e_i as it's nearest neighbor. $N_i^{(0)}$ is initially set as zero.

A.2 Codebook Clustering of Model-based RAQ-VAE

Given a set of the original codebook representations $\mathbf{e} = \{e_i\}_{i=1}^K$, we aim to partition the K code vectors into $\tilde{K} (\leq K)$ code vectors $\tilde{\mathbf{e}} = \{\tilde{e}_i\}_{i=1}^{\tilde{K}}$. Each codebook vector resides in a D -dimensional Euclidean space. Using the codebook assignment function $g(\cdot)$, then $g(e_i) = j$ means i -th given codebook assigned j -th clustered codebook. Our objective for codebook clustering is to minimize the discrepancy \mathcal{L} between the given codebook \mathbf{e} and clustered codebook $\tilde{\mathbf{e}}$:

$$\arg \min_{\tilde{\mathbf{e}}, g} \mathcal{L}(\mathbf{e}; \tilde{\mathbf{e}}) = \arg \min_{\tilde{\mathbf{e}}, g} \sum_{i=1}^{\tilde{K}} \|e_i - \tilde{e}_{g(e_i)}\| \tag{7}$$

with necessary conditions

$$g(e_i) = \arg \min_{j \in \{1, 2, \dots, \tilde{K}\}} \|e_i - \tilde{e}_j\|, \quad \tilde{e}_j = \frac{\sum_{i: g(e_i)=j} e_i}{N_j} \tag{8}$$

where N_j is the number of samples assigned to the codebook \tilde{e}_j .

A.3 Experiment Details

A.3.1 Architectures and Hyperparameters

The model architecture for this study is based on the conventional VQ-VAE framework outlined in the original VQ-VAE paper [48], and is implemented with reference to the VQ-VAE-2 [40] implementation repositories^{2,3,4}. We are using the ConvResNets from the repositories. These networks consist of convolutional layers, transpose convolutional layers and ResBlocks. Experiments were conducted on two different computer setups: a server with 4 RTX 4090 GPUs and a machine with 2 RTX 3090 GPUs. PyTorch [37], PyTorch Lightning [12], and the AdamW [31] optimizer were used for model implementation and training. Evaluation metrics such as the Structural Similarity Index (SSIM) and the Fréchet Inception Distance (rFID) were computed using implementations of pytorch-msssim⁵ and pytorch-fid⁶, respectively. The detailed model parameters are shown in Table 1. RAQ-VAEs are constructed based on the described VQ-VAE parameters with additional consideration of each parameter.

A.3.2 Datasets and Preprocessing

For the **CIFAR10** dataset, the training set is preprocessed using a combination of random cropping and random horizontal flipping. Specifically, a random crop of size 32×32 with padding of 4 using the 'reflect' padding mode is applied, followed by a random horizontal flip. The validation and test sets are processed by converting the images to tensors without further augmentation. For the **CelebA** dataset, the training set is preprocessed with a series of transformations. The images are resized

²<https://github.com/mattiasxu/VQVAE-2>

³<https://github.com/rosinality/vq-vae-2-pytorch>

⁴<https://github.com/EugenHotaj/pytorch-generative>

⁵<https://github.com/VainF/pytorch-msssim>

⁶<https://github.com/mseitzer/pytorch-fid>

Table 1: Architecture and hyperparameters of baseline VQ-VAE model and its RAQ-VAE model (Model-based RAQ-VAE and Data-driven RAQ-VAE)

Method	Parameter	CIFAR10	CelebA	ImageNet
VQ-VAE [48]	Input size	$32 \times 32 \times 3$	$64 \times 64 \times 3$	$224 \times 224 \times 3$
	Latent layers	8×8	16×16	56×56
	Hidden units	128	128	256
	Residual units	64	64	128
	# of ResBlock	2	2	2
	Original codebook size (K)	$2^4 \sim 2^{10}$	$2^5 \sim 2^{11}$	$2^7 \sim 2^{12}$
	Codebook dimension (D)	64	64	128
	β (Commit loss weight)	0.25	0.25	0.25
	Weight decay in EMA (γ)	0.99	0.99	0.99
	Batch size	128	128	32
	Optimizer	AdamW	AdamW	AdamW
	Learning rate	0.0005	0.0005	0.0005
	Max. training steps	195K	635.5K	2500K
Model-based RAQ-VAE	Original codebook size (K)	64, 128	128, 256	512
	Adapted codebook size (\tilde{K})	$2^4 \sim 2^{10}$	$2^5 \sim 2^{11}$	$2^6 \sim 2^{12}$
	Max. DKM iteration	200	200	200
	Max. IKM iteration	5000	5000	5000
	τ of softmax	0.01	0.01	0.01
Data-driven RAQ-VAE	Original codebook size (K)	64, 128	128, 256	512
	Adapted codebook size (\tilde{K})	$2^4 \sim 2^{10}$	$2^5 \sim 2^{11}$	$2^6 \sim 2^{12}$
	Max. Codebook size	1024	2048	4096
	Min. Codebook size	8	16	64
	Input size (Seq2Seq)	64	64	128
	Hidden size (Seq2Seq)	64	64	128
# of recurrent layers (Seq2Seq)	2	2	2	

and center cropped to 64×64 , normalized, and subjected to random horizontal flipping. A similar preprocessing is applied to the validation set, while the test set is processed without augmentation. For the **ImageNet** dataset, the training set is preprocessed with a series of transformations. The images are resized 256×256 and center cropped to 224×224 , normalized, and subjected to random horizontal flipping. A similar preprocessing is applied to the validation set, while the test set is processed without augmentation. These datasets are loaded into PyTorch using the provided data modules, and the corresponding data loaders are configured with the specified batch sizes and learning rate for efficient training (described in Table 1. The datasets are used as input for training, validation, and testing of the VQ-VAE model.

A.3.3 Model Complexity

To provide a comprehensive understanding of the model complexity for the different datasets used in our experiments, we detail the number of parameters in the Encoder, Decoder, Quantizer, and Seq2Seq components of the trained models in Table 2 and 3. The table below summarizes the number of model parameters counts for the CIFAR10 and CelebA datasets.

Table 2: Number of parameters for training our models on CIFAR10 dataset.

Method	# params				Total
	Encoder	Decoder	Quantizer	Seq2Seq	
VQ-VAE ($K = 1024$)	196.3K	262K	65.5 K	-	525K
VQ-VAE ($K = 512$)	196.3K	262K	32.8K	-	492K
VQ-VAE ($K = 256$)	196.3K	262K	16.4K	-	476K
VQ-VAE ($K = 128$)	196.3K	262K	8.2K	-	468K
VQ-VAE ($K = 64$)	196.3K	262K	4.1K	-	463K
VQ-VAE ($K = 32$)	196.3K	262K	2.0K	-	461K
VQ-VAE ($K = 16$)	196.3K	262K	1.0K	-	460K
VQ-VAE ($K = 1024$) (randomly selected codebook)	196.3K	262K	65.5 K	-	525K
Data-driven RAQ-VAE ($K = 128$)	196.3K	262K	8.2K	263.7K	732K
Data-driven RAQ-VAE ($K = 64$)	196.3K	262K	4.1K	263.7K	728K
Model-based RAQ-VAE ($K = 128$)	196.3K	262K	8.2K	-	468K
Model-based RAQ-VAE ($K = 64$)	196.3K	262K	4.1K	-	463K

Table 3: Number of parameters for training our models on CelebA dataset.

Method	# params				Total
	Encoder	Decoder	Quantizer	Seq2Seq	
VQ-VAE ($K = 2048$)	196.3K	262K	131K	-	590K
VQ-VAE ($K = 1024$)	196.3K	262K	65.5 K	-	525K
VQ-VAE ($K = 512$)	196.3K	262K	32.8K	-	492K
VQ-VAE ($K = 256$)	196.3K	262K	16.4K	-	476K
VQ-VAE ($K = 128$)	196.3K	262K	8.2K	-	468K
VQ-VAE($K = 64$)	196.3K	262K	4.1K	-	463K
VQ-VAE ($K = 32$)	196.3K	262K	2.0K	-	461K
VQ-VAE ($K = 2048$) (randomly selected codebook)	196.3K	262K	131K	-	590K
Data-driven RAQ-VAE ($K = 256$)	196.3K	262K	16.4K	263.7K	740K
Data-driven RAQ-VAE ($K = 128$)	196.3K	262K	8.2K	263.7K	732K
Model-based RAQ-VAE ($K = 256$)	196.3K	262K	16.4K	-	476K
Model-based RAQ-VAE ($K = 128$)	196.3K	262K	8.2K	-	468K

A.4 Additional Experiments

A.4.1 Reducing the Rate

As analyzed in Section 5.1, data-driven RAQ-VAE generally outperforms model-based RAQ-VAE, but some rate-reduction results on CIFAR10 show that model-based RAQ-VAE performs much more stably than in the codebook increasing task. This indicates that simply clustering codebook vectors, without additional neural models like Seq2Seq, can achieve remarkable performance.

In Table 4, the performance via codebook clustering was evaluated with different original/adapted codebook sizes K : 1024 / \tilde{K} : 512, 256, 128 on CIFAR10 and K : 2048 / \tilde{K} : 1024, 512, 256, 128 on CelebA. The conventional VQ-VAE preserved as many codebooks in the original codebook as in the adapted codebook, while randomly codebook-selected VQ-VAE results remained meaningless. Model-based RAQ-VAE adopted this baseline VQ-VAE model and performed clustering on the adapted codebook. Model-based RAQ-VAE shows a substantial performance difference in terms of reconstructed image distortion and codebook usage compared to randomly codebook-selected VQ-VAE. Even when evaluating absolute performance, it is intuitive that online codebook representation via model-based RAQ-VAE provides some performance guarantees.

Table 4: Reconstruction performances for **rate-reduction task** according to adapted codebook size \tilde{K} . The distortion (PSNR), perceptual similarity (rFID), and codebook usability (perplexity) are evaluated using the test set on CIFAR-10 and CelebA. Higher values are better for PSNR, and perplexity, while lower values are better for rFID.

Method	\tilde{K}	CIFAR10 ($K = 1024$)		
		PSNR \uparrow	rFID \downarrow	Perplexity \uparrow
VQ-VAE (baseline model)	-	25.48	51.90	708.60
VQ-VAE (random select)	512	24.35	63.67	289.29
	256	22.81	78.00	111.77
	128	20.87	93.57	48.87
Model-based RAQ-VAE	512	24.62	55.78	285.68
	256	23.81	62.53	134.54
	128	23.07	69.45	73.17

Method	\tilde{K}	CelebA ($K = 2048$)		
		PSNR \uparrow	rFID \downarrow	Perplexity \uparrow
VQ-VAE (baseline model)	-	28.26	22.89	273.47
VQ-VAE (random select)	1024	24.02	38.92	103.50
	512	18.99	71.64	49.59
	256	23.54	115.12	27.86
Model-based RAQ-VAE	1024	26.40	31.37	102.36
	512	25.24	39.07	53.45
	256	24.36	45.54	32.86

A.4.2 Increasing the Rate

In our proposed RAQ-VAE scenario, increasing the codebook size beyond the base size is a more demanding and crucial task than reducing it. The crucial step in building data-driven RAQ-VAE is to achieve higher rates from a fixed model architecture and compression rate, ensuring usability. Therefore, the codebook increasing task was the main challenge. The Seq2Seq decoding algorithm based on cross-forcing is designed with this intention.

In Figure 2, the codebook generation performance was evaluated with different original/adapted codebook sizes K : 64, 128 / \tilde{K} : 64, 128, 256, 512, 1024 on CIFAR10 and K : 128, 256 / \tilde{K} : 128, 256, 512, 1024, 2048 on CelebA datasets. As discussed in Section 5.1, data-driven RAQ-VAE outperforms model-based RAQ-VAE in the rate-increasing task and partially outperforms conventional VQ-VAE trained on the same codebook size ($K = \tilde{K}$). This effect is particularly pronounced on CelebA.

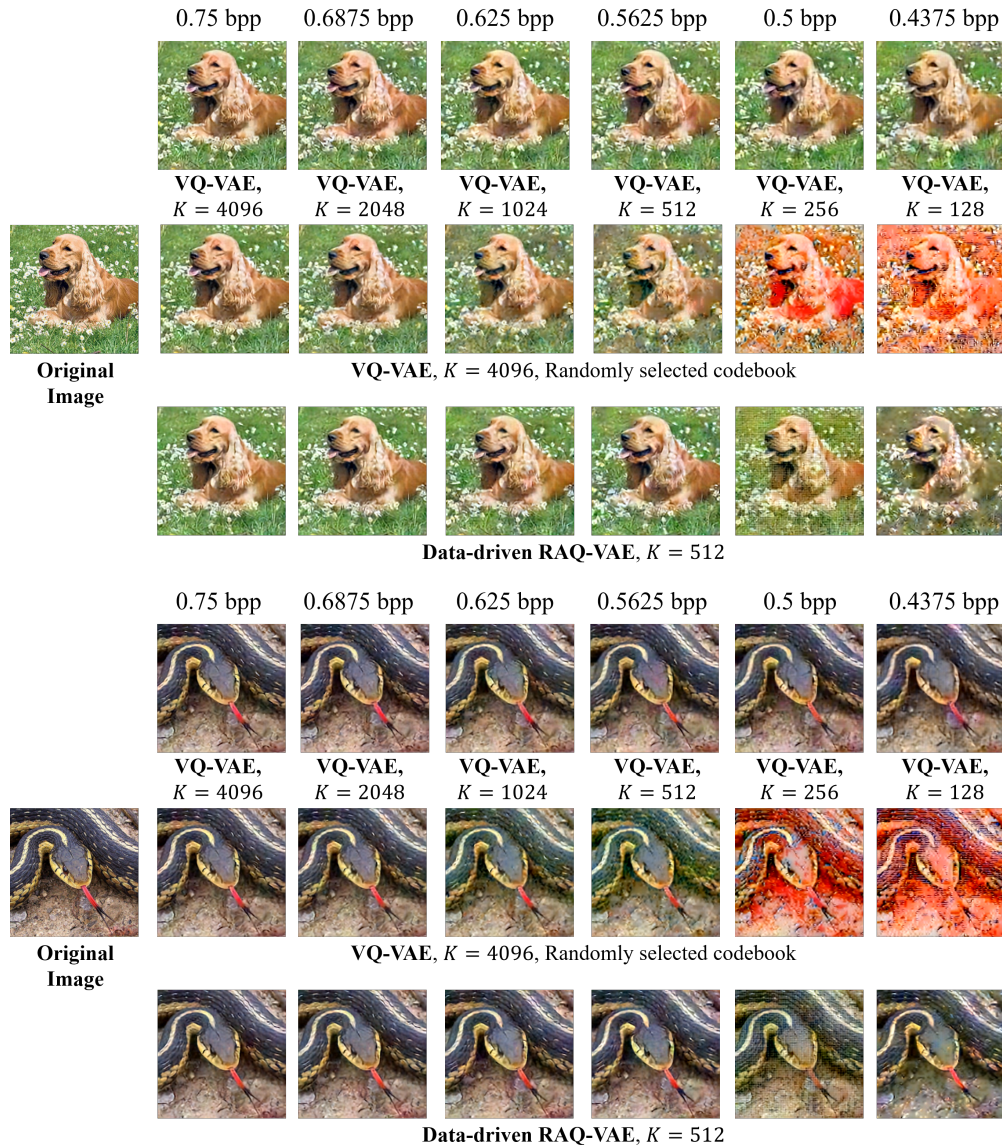


Figure 5: **Reconstructed images** for ImageNet dataset at different rates.

However, increasing the difference between the original and adapted codebook sizes leads to a degradation of RAQ-VAE performance. This effect is more dramatic for model-based RAQ-VAE due to its algorithmic limitations, making its performance less stable at high rates. Improving the performance of model-based RAQ-VAE, such as modifying the initialization of the codebook vector, remains a limitation.

A.4.3 Additional Qualitative Results

In Figure 5, we present additional qualitative results for the reconstruction on ImageNet dataset.

A.4.4 Additional Quantitative Results

In Table 5 and 6, we present additional quantitative results for the reconstruction on CIFAR10 and CelebA datasets. The error indicates a 95.45% confidence interval based on 4 runs with different training seeds.

Table 5: **Reconstruction performance** on CIFAR10 dataset. The 95.45% confidence interval is provided based on 4 runs with different training seeds.

Method	Bit Rate	Codebook Usability		Distortion	Perceptual Similarity	
	\tilde{K} (bpp)	Usage	Perplexity	PSNR	rFID	SSIM
VQ-VAE ($K = \tilde{K}$)	1024 (0.625)	972.66±2.97	708.60±7.04	25.48±0.02	51.90±0.51	0.8648±0.0005
VQ-VAE ($K = \tilde{K}$)	512 (0.5625)	507.52±0.51	377.08±5.92	24.94±0.01	56.65±0.91	0.8490±0.0003
VQ-VAE ($K = \tilde{K}$)	256 (0.5)	256±0	204.43±4.36	24.43±0.02	61.40±0.78	0.8310±0.0006
VQ-VAE ($K = \tilde{K}$)	128 (0.4375)	128±0	106.44±1.54	23.85±0.01	66.70±1.12	0.8096±0.0009
VQ-VAE ($K = \tilde{K}$)	64 (0.375)	64±0	55.64±0.27	23.24±0.01	74.00±1.64	0.7849±0.0009
VQ-VAE ($K = \tilde{K}$)	32 (0.3125)	32±0	29.25±0.13	22.53±0.02	81.68±1.01	0.7545±0.0009
VQ-VAE ($K = \tilde{K}$)	16 (0.25)	16±0	15.01±0.21	21.76±0.01	89.75±0.83	0.7156±0.0024
VQ-VAE ($K = 1024$) (random select)	1024 (0.625)	972.66±2.97	708.60±7.04	25.48±0.02	51.90±0.51	0.8648±0.0005
	512 (0.5625)	498.38±1.85	289.29±16.67	24.35±0.11	63.67±2.49	0.8305±0.0056
	256 (0.5)	253.01±0.66	111.77±21.53	22.81±0.38	78.00±5.07	0.7822±0.0100
	128 (0.4375)	127.34±0.33	48.87±11.31	20.87±0.73	93.57±9.87	0.7254±0.0235
	64 (0.375)	64±0	24.31±5.26	19.46±0.98	109.90±14.20	0.6720±0.0309
	32 (0.3125)	32±0	13.50±1.45	17.76±1.12	126.57±15.89	0.6102±0.0350
Data-driven RAQ-VAE ($K = 128$)	1024(0.625)	971.21±4.14	724.91±15.34	24.85±0.02	57.03±1.34	0.8420±0.0008
	512 (0.5625)	503.48±0.75	380.02±6.82	24.57±0.02	59.36±0.62	0.8326±0.0008
	256 (0.5)	253.45±0.50	194.27±2.38	24.12±0.02	62.18±1.09	0.8193±0.0009
	128 (0.4375)	128±0	109.65±3.50	23.71±0.01	66.89±1.07	0.8071±0.0014
	64 (0.375)	64±0	55.64±0.27	23.08±0.02	71.84±0.31	0.7855±0.0005
	32 (0.3125)	32±0	29.50±0.21	21.76±0.06	82.85±0.87	0.7384±0.0007
Model-based RAQ-VAE ($K = 128$)	16 (0.25)	16±0	15.11±0.67	20.79±0.18	104.86±5.91	0.6918±0.0084
	1024 (0.625)	744.36±18.74	395.23±2.77	24.15±0.03	63.88±1.26	0.8213±0.0014
	512 (0.5625)	430.06±11.58	256.23±7.50	24.04±0.03	64.74±0.96	0.8177±0.0012
	256 (0.5)	244.61±3.13	185.02±3.31	23.93±0.01	65.65±1.12	0.8139±0.0010
	128 (0.4375)	128±0	106.44±1.54	23.85±0.01	66.70±1.12	0.8096±0.0009
	64 (0.375)	64±0	49.55±1.29	22.85±0.55	72.61±0.77	0.7780±0.0013
Data-driven RAQ-VAE ($K = 64$)	32 (0.3125)	32±0	25.65±0.76	21.88±0.75	82.12±1.74	0.7405±0.0046
	16 (0.25)	16±0	13.79±0.06	20.89±0.04	95.03±0.34	0.6972±0.0010
	1024 (0.625)	972.14±6.49	725.55±10.90	25.04±0.01	55.34±1.48	0.8487±0.0012
	512 (0.5625)	506.38±1.23	382.43±10.58	24.70±0.02	57.91±1.42	0.8387±0.0011
	256 (0.5)	255.52±0.48	196.17±9.95	24.25±0.02	61.96±1.00	0.8245±0.0012
	128 (0.4375)	128±0	109.65±3.50	23.71±0.01	66.89±1.07	0.8071±0.0014
Model-based RAQ-VAE ($K = 64$)	64 (0.375)	64±0	56.31±0.46	23.23±0.01	71.17±1.17	0.7897±0.0013
	32 (0.3125)	32±0	29.62±0.66	21.84±0.09	90.04±1.44	0.7350±0.0038
	16 (0.25)	16±0	15.11±0.67	20.79±0.18	104.86±5.91	0.6918±0.0084
	1024 (0.625)	706.20±115.18	345.50±107.06	23.65±0.13	70.30±2.02	0.8013±0.0051
	512 (0.5625)	428.39±12.29	231.41±14.64	23.55±0.04	71.01±1.38	0.7988±0.0005
	256 (0.5)	233.75±4.63	140.19±2.82	23.39±0.05	71.72±1.43	0.7935±0.0012
Model-based RAQ-VAE ($K = 64$)	128 (0.4375)	125.07±1.58	101.16±16.04	23.32±0.05	72.68±1.47	0.7901±0.0008
	64 (0.375)	64±0	55.64±0.27	23.24±0.01	74.00±1.64	0.7849±0.0009
	32 (0.3125)	32±0	26.21±0.95	22.07±0.13	81.61±2.26	0.7569±0.0014
	16 (0.25)	16±0	13.59±0.85	20.88±0.23	92.84±3.30	0.7004±0.0063

Table 6: **Reconstruction performance** on CelebA dataset. The 95.45% confidence interval is provided based on 4 runs with different training seeds.

Method	Bit Rate	Codebook Usability		Distortion	Perceptual Similarity	
	\tilde{K} (bpp)	Usage	Perplexity	PSNR	rFID	SSIM
VQ-VAE ($K = \tilde{K}$)	2048 (0.6875)	779.07±8.35	273.47±6.86	28.26±0.03	22.89±0.71	0.8890±0.0027
VQ-VAE ($K = \tilde{K}$)	1024 (0.625)	456.86±3.53	160.35±2.73	27.73±0.05	26.67±1.43	0.8763±0.0029
VQ-VAE ($K = \tilde{K}$)	512 (0.5625)	259.59±3.99	95.09±1.28	27.11±0.01	29.77±0.95	0.8636±0.0022
VQ-VAE ($K = \tilde{K}$)	256 (0.5)	144.44±2.49	57.86±0.91	26.46±0.03	31.53±1.01	0.8481±0.0009
VQ-VAE ($K = \tilde{K}$)	128 (0.4375)	80.26±0.99	34.98±0.39	25.72±0.04	36.25±0.98	0.8279±0.0027
VQ-VAE ($K = \tilde{K}$)	64 (0.375)	44.94±1.03	20.04±0.37	24.78±0.03	41.22±0.77	0.7986±0.0037
VQ-VAE ($K = \tilde{K}$)	32 (0.3125)	25.48±0.69	12.69±0.31	23.76±0.06	46.56±1.97	0.7660±0.0032
VQ-VAE ($K = 2048$) (random select)	2048 (0.625)	779.07±8.35	273.47±6.86	28.26±0.03	22.89±0.71	0.8890±0.0027
	1024 (0.5625)	384.31±6.76	103.50±3.28	24.02±1.10	38.92±3.27	0.7963±0.0201
	512 (0.5)	210.69±9.23	49.59±4.54	18.99±1.40	71.64±8.27	0.7037±0.0221
	256 (0.4375)	115.33±7.73	27.86±3.39	16.33±0.61	115.12±11.93	0.6353±0.0173
Data-driven RAQ-VAE ($K = 256$)	2048 (0.625)	885.53±6.76	347.99±5.17	27.96±0.14	23.02±0.33	0.8858±0.0033
	1024 (0.5625)	490.86±4.98	187.33±10.37	27.51±0.13	25.08±0.23	0.8758±0.0036
	512 (0.5)	275.84±1.72	104.61±5.00	26.95±0.086	27.96±0.49	0.8637±0.0045
	256 (0.4375)	144.79±1.21	52.63±0.28	26.29±0.054	32.34±0.86	0.8463±0.0030
	128 (0.375)	80.21±4.27	32.23±3.87	25.13±0.26	39.67±2.29	0.8162±0.0071
	64 (0.3125)	42.93±1.61	20.85±1.22	24.09±0.21	51.57±6.66	0.7912±0.0094
	32 (0.25)	22.76±1.57	12.32±0.91	22.62±0.27	69.65±9.49	0.7479±0.0129
Model-based RAQ-VAE ($K = 256$)	2048 (0.625)	704.17±108.04	117.53±33.57	26.54±0.10	30.34±1.39	0.8507±0.0041
	1024 (0.5625)	460.77±26.98	134.48±11.26	26.59±0.06	30.49±1.10	0.8509±0.0021
	512 (0.5)	279.53±9.48	100.64±08.94	26.40±0.08	30.95±0.98	0.8488±0.0017
	256 (0.4375)	144.44±2.49	57.86±0.91	26.46±0.03	31.53±1.01	0.8481±0.0009
	128 (0.375)	75.31±3.09	25.05±1.95	24.44±0.25	38.95±2.91	0.7890±0.0141
	64 (0.3125)	41.66±1.22	14.73±0.56 3	22.85±0.36	48.96±1.13	0.7391±0.0192
	32 (0.25)	22.96±0.90	10.16±0.95	21.81±0.45	62.46±0.00	0.7077±0.0195
Data-driven RAQ-VAE ($K = 128$)	2048 (0.625)	891.13±7.11	345.25±5.15	27.91±0.04	22.64±0.76	0.8810±0.0013
	1024 (0.5625)	490.15±14.39	176.71±6.19	27.47±0.07	24.67±0.80	0.8710±0.0016
	512 (0.5)	272.60±2.08	96.87±2.68	26.90±0.05	26.90±0.04	0.8589±0.0044
	256 (0.4375)	152.65±2.45	60.90±2.18	26.18±0.18	30.81±1.59	0.8391±0.0125
	128 (0.375)	79.17±0.93	31.36±0.77	25.53±0.06	36.30±1.12	0.8209±0.0072
	64 (0.3125)	42.71±1.66	19.78±2.31	24.10±0.11	47.63±5.82	0.7892±0.0067
	32 (0.25)	22.42±1.92	11.43±2.14	22.74±0.54	62.39±3.76	0.7414±0.0304
Model-based RAQ-VAE ($K = 128$)	2048 (0.625)	350.02±100.57	64.87±21.22	22.77±0.78	52.37±10.94	0.7463±0.0347
	1024 (0.5625)	432.15±45.80	102.79±17.34	25.57±0.19	35.62±1.46	0.8296±0.0062
	512 (0.5)	262.78±29.47	75.63±12.04	25.50±0.29	36.82±0.73	0.8265±0.0026
	256 (0.4375)	153.16±5.46	53.22±4.62	25.42±0.28	36.78±1.27	0.8285±0.0022
	128 (0.375)	80.26±0.99	34.98±0.39	25.72±0.04	36.25±0.98	0.8279±0.0027
	64 (0.3125)	41.88±0.72	16.70±0.43	23.63±0.16	47.09±4.09	0.7736±0.0080
	32 (0.25)	23.31±0.89	9.56±0.77	21.64±0.13	64.85±6.92	0.7037±0.0102